iScience

CellPress
OPEN ACCESS

Article

Phytophthora sojae leucine-rich repeat receptor-like kinases: diverse and essential roles in development and pathogenicity

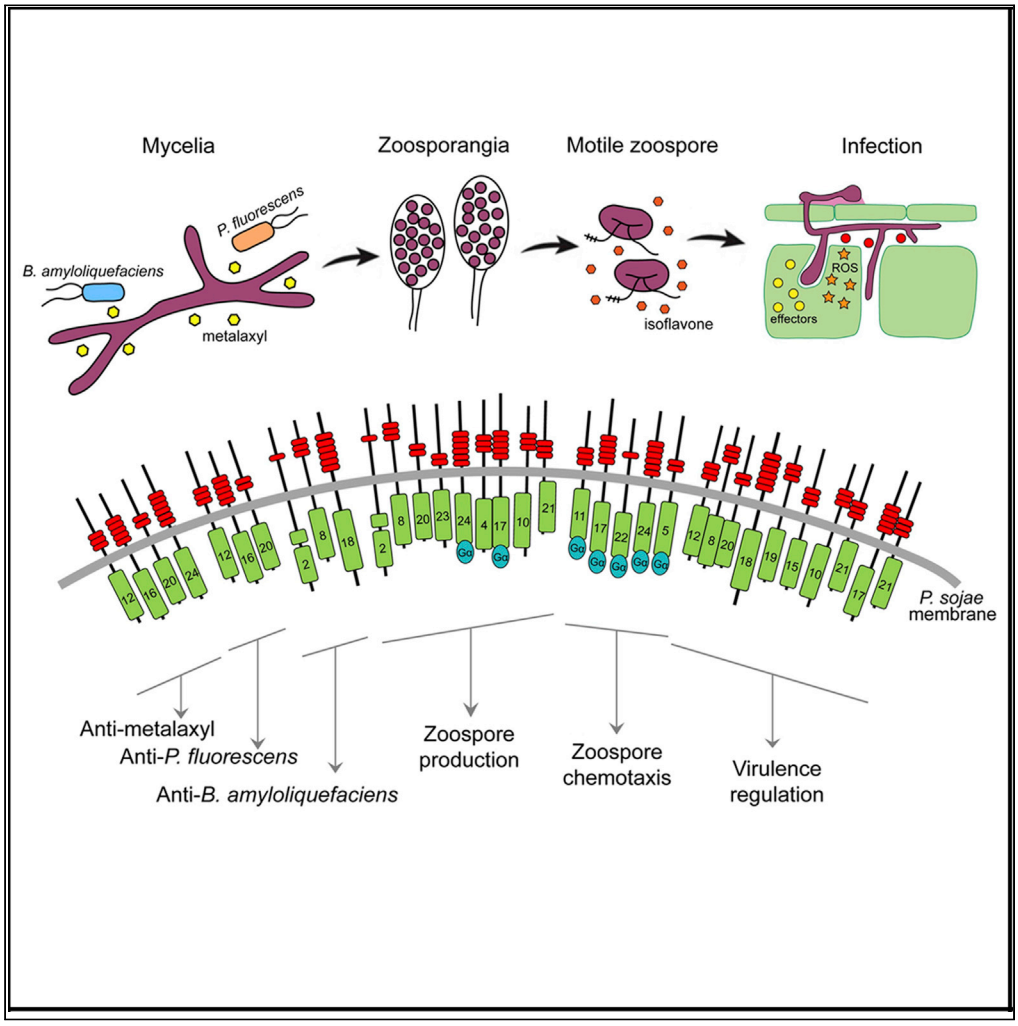

Jierui Si, Yong Pei, Danyu Shen, ..., Hao Peng, Xiangxiu Liang, Daolong Dou

ddou@njau.edu.cn

Highlights

Systematically functional analysis of LRR-RLK family with 24 members in *P. sojae*

Five chemotaxis-related PsRLKs directly interact with Gα protein PsGPA1

PsRLKs form an interaction network in *P. sojae*

The complex PsRLK21-PsRLK10/17 jointly regulates pathogenesis

Si et al., iScience *24*, 102725
July 23, 2021
https://doi.org/10.1016/j.isci.2021.102725

iScience

CellPress
OPEN ACCESS

Article

Phytophthora sojae leucine-rich repeat receptor-like kinases: diverse and essential roles in development and pathogenicity

Jierui Si,[1,4] Yong Pei,[1,4] Danyu Shen,[1] Peiyun Ji,[1] Ruofei Xu,[1] Xue Xue,[1] Hao Peng,[2] Xiangxiu Liang,[3] and Daolong Dou[1,3,5,*]

SUMMARY

Leucine-rich repeat receptor-like kinases (LRR-RLKs) are critical signal receptors in plant development and defense. Like plants, oomycete pathogen genomes also harbor LRR-RLKs, but their functions remain largely unknown. Here, we systematically characterize all the 24 *LRR-RLK* genes (*PsRLKs*) from *Phytophthora sojae*, which is a model of oomycete pathogens. Although none of them was required for vegetative growth, the specific PsRLKs are important for stress responses, zoospore production, zoospores chemotaxis, and pathogenicity. Interestingly, the Gα subunit PsGPA1 interacts with the five chemotaxis-related PsRLKs via their intracellular kinase domains, and expression of *PsGPA1* gene is downregulated in the three mutants (Δ*PsRLK17/22/24*). Moreover, we generated the PsRLK-PsRLK interaction network of *P. sojae* and found that PsRLK21, together with PsRLK10 or PsRLK17, regulate virulence by direct association. Taken together, our results reveal the diverse roles of LRR-RLKs in modulating *P. sojae* development, interaction with soybean, and responses to diverse environmental factors.

INTRODUCTION

Almost all living organisms evolve sensory proteins to perceive environmental signals and communicate them across cells (van der Geer et al., 1994). The leucine-rich repeat receptor-like protein kinases (LRR-RLKs) represent one of the most important sensory protein families that play crucial roles in plant growth, development, and stress responses (Diévart and Clark, 2003; Shiu and Bleecker, 2001a; Shiu and Bleecker, 2003). Widely distributed in plants, LRR-RLKs have expanded to hundreds of members in each genome (Fischer et al., 2016; Magalhaes et al., 2016; Shiu and Bleecker, 2001b). A typical plant LRR-RLK consists of three functional domains. The N-terminal extracellular domain (ECD) comprises varying numbers of LRRs that provide binding sites for the sense of a wide array of endogenous and exogenous ligands including peptides and small hormone molecules. The transmembrane domain (TM) functions as an anchor, while the intracellular kinase domain (KD) interacts and phosphorylates proteins of downstream signal pathways (Gou et al., 2010; Shiu and Bleecker, 2001a; Song et al., 2017).

The functions of multiple plant LRR-RLKs have been well-investigated. For example, brassinosteroid insensitive1 (BRI1) perceives the steroid hormones brassinosteroids (BRs) and is essential for diverse plant growth and development processes (Nolan et al., 2017). *Arabidopsis thaliana* FLAGELLIN SENSING 2 (FLS2) perceives bacterial flagellin (flg22) to activate the defense responses against pathogens via association with BRI1-associated receptor kinase 1 (BAK1). BAK1 is also known as somatic embryogenesis receptor kinase 3 and acts as a coreceptor for several other LRR-RLKs (Chinchilla et al., 2007). Defense-signaling LRR-RLKs couple with G proteins, NADPH oxidase respiratory burst oxidase homolog D, and other regulatory components to form a large and dynamic immune receptor complex (Chinchilla et al., 2009; Tang et al., 2017).

Neither animals nor fungi possess canonical LRR-RLKs despite the existence of closely related Toll-like receptor (TLR) proteins in some animals (Diévart et al., 2011). Each TLR protein is structurally similar to LRR-RLK, contains LRRs, a TM and an intracellular Toll/IL -1 receptor (TIR) domain, is usually involved in animal development and immunity (O'Neill, 2004). Interestingly, LRR-RLKs are not plant-specific because some nonplant members have been bioinformatically identified in *Monosiga brevicollis* (a choanoflagellate),

[1]Key Laboratory of Plant Immunity, College of Plant Protection, Academy for Advanced Interdisciplinary Studies, Nanjing Agricultural University, Nanjing 210095, China

[2]Department of Crop and Soil Sciences, Washington State University, Pullman, WA 99164-6420, USA

[3]Key Laboratory of Pest Monitoring and Green Management, MOA and College of Plant Protection, China Agricultural University, Beijing 100193, China

[4]These authors contributed equally

[5]Lead contact

*Correspondence: ddou@njau.edu.cn

https://doi.org/10.1016/j.isci.2021.102725

Chlorella variabilis (a green alga), *Ectocarpus siliculosus* (a brown alga), and oomycetes (Diévart et al., 2011). However, the biological functions of these nonplant LRR-RLKs are still largely unknown.

All known oomycetes possess varying numbers of LRR-RLKs, which share a similar domain structure with well-studied plant LRR-RLKs (Diévart et al., 2011; Soanes and Talbot, 2010). Expressed sequence tag analysis reveals that oomycete LRR-RLK-encoding genes are expressed during vegetative growth and host infection [14]. We recently reported that PcLRR-RK1 functions in *Phytophthora capsici* virulence and development of mycelium, sporangia, and zoospores (Safdar et al., 2017). Only one to two RLKs can be found in species such as *Hyaloperonospora parasitica* and *Pythium ultimum*. In contrast, several duplication events occurred independently in *Saprolegnia* and *Phytophthora* species (Diévart et al., 2011). Consequently, the fish pathogen *Saprolegnia parasitica* has an expanded number of 34 LRR-RLKs. Meanwhile, 20 to 25 LRR-RLKs can be found in *Phytophthora* species, such as *Phytophthora sojae*, *Phytophthora infestans,* and *Phytophthora ramorum* (Diévart et al., 2011).

Phytophthora species are fungal-like organisms and belong to the kingdom Stramenopila, which constitutes a distinct and major branch in the eukaryotic evolutionary tree and comprises diatoms, kelp saprophytes and pathogens infecting plants, animals, or insects (Gunderson et al., 1987; Thines, 2014). Most *Phytophthora* species are notorious plant-infecting pathogens that cause devastating diseases on a wide range of crops (Jiang and Tyler, 2012). In particular, *P. sojae* is an economically important soybean-infecting pathogen that threatens global soybean production by causing root and stem rot diseases. Owing to the availability of abundant genomic data (Tyler et al., 2006; Ye et al., 2011) and well-established gene editing technique (Fang and Tyler, 2016), *P. sojae* has emerged as a model for studying the molecular basis of oomycete development and pathogenesis (Tyler, 2007; Tyler et al., 2006).

Similar to many other oomycete pathogens, *P. sojae* has developed a diverse lifestyle and evolved sophisticated mechanisms to escape or suppress host immunity and overcome oomyceticides (Cohen and Coffey, 1986; Judelson and Ah-Fong, 2019; Tyler, 2007). It normally starts infection and colonization as asexual sporangium-derived zoospores. Specifically attracted by isoflavones daidzein exuded via soybean roots (Morris et al., 1998; Morris and Ward, 1992; Tyler, 2007), zoospores swim toward host and form germ tubes to penetrate the roots. Zoospore behavior and chemotaxis rely on G-protein α subunit PsGPA1 (Hua et al., 2008). It was reported that PsGPA1 acts as a negative regulator of sporangium formation by physically inhibiting the nuclear localization of a serine-threonine kinase protein PsYPK1 (Qiu et al., 2020), and histidine triad nucleotide-binding protein 1 (PsHint1) also interacts with PsGPA1 to regulate zoospore chemotaxis, cyst germination, and virulence (Zhang et al., 2016).

The mechanism for potential upstream regulation of PsGPA1 remains elusive. Because G proteins couple with RLKs to mediate immunity responses in plants, it is possible to infer that similar pathways may also exist in oomycetes (Liang et al., 2016; Nitta et al., 2015). To test this hypothesis, we systematically investigate the functions of *P. sojae* LRR-RLKs (PsRLKs) by generating the protein interaction network and creating CRISPR/Cas9-mediated gene knockout mutants for all the 24 PsRLKs identified. Genetic analysis of these mutants demonstrates the differential roles of individual PsRLKs in sporangia formation, zoospore chemotaxis, virulence, and stress response. Five PsGPA1-interacting PsRLKs (PsRLK5/11/17/22/24) affect zoospore chemotaxis with three of them (PsRLK17/22/24) involved the regulation of *PsGPA1* expression. Among virulence-related PsRLKs, PsRLK20 interacts with PsRLK17 or PsRLK10 to jointly regulate virulence. Taken together, our findings for the first time dissect the diverse and overlapping roles of LRR-RLKs in *P. sojae* development, stress response, and pathogenesis. We also reveal their interaction features including self-association and forming receptor complex with G protein.

RESULTS

LRR-RLK family is independently evolved in oomycetes

A total of 3–24 *LRR-RLK* genes were identified in each detected oomycete genome by filtering encoded proteins containing the predicted TM, KD, and at least one LRR motif in ECD (Figure 1A). This is a much smaller group compared to hundreds of LRR-RLKs identified in plant genomes. In contrast, no LRR-RLK protein was identified in diatoms, fungi, or metazoan, whereas numbers of TLR proteins containing LRR, TM, and TIR were found in metazoan (Figure 1A). A phylogenetic tree was constructed using all LRR-RLKs from 6 selected oomycete genomes and a representative member of each subgroup LRR-RLKs from *A. thaliana*. The two distinct clades belonging to *A. thaliana* and oomycetes, respectively, were clearly observed in the tree

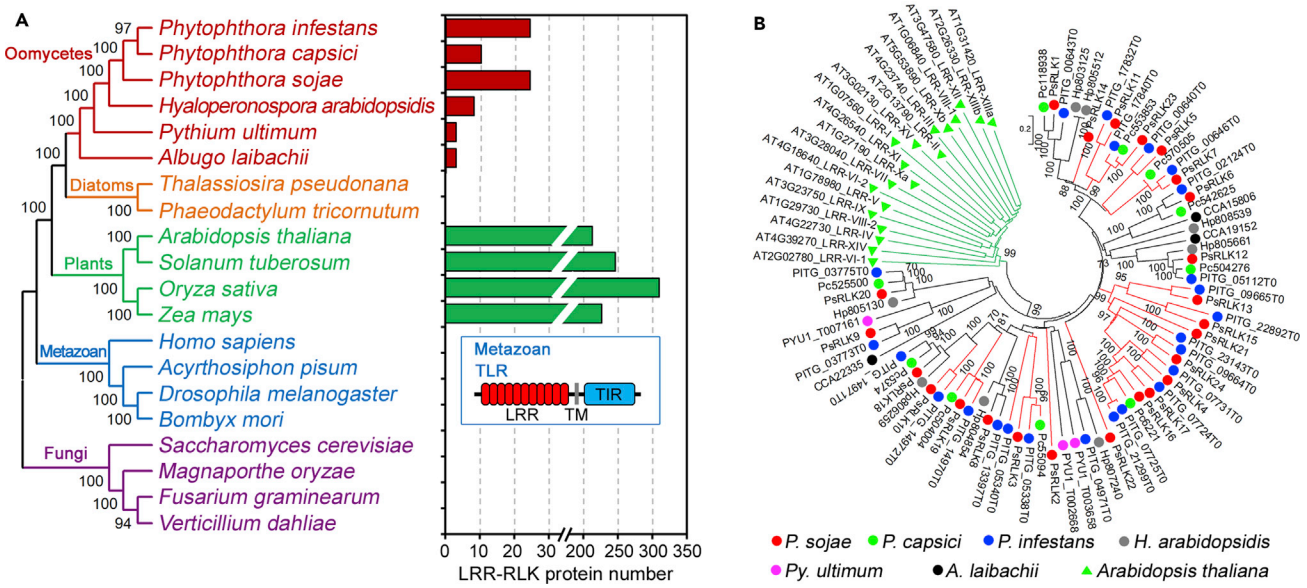

Figure 1. LRR-RLKs are independently evolved in oomycetes

(A) Comparison of LRR-RLK numbers in representative subsets of oomycetes, diatoms, plants, metazoan, and fungi.

(B) Phylogenetic analysis of oomycete and representative *A. thaliana* LRR-RLKs. The phylogenetic tree was constructed using all the identified oomycete LRR-RLKs together with the selected *A. thaliana* LRR-RLKs belonging to different subgroup. The red dots represent *Phytophthora*-specific LRR-RLKs. More detail information was shown in Figures S1–S3.

(Figure 1B), suggestive of independent evolution of LRR-RLKs in oomycetes and *A. thaliana*. Moreover, in the oomycete-specific clade, several branches only contained LRR-RLKs derived from *P. sojae, P. infestans*, and *P. capsici* (Figure 1B), indicating that LRR-RLKs were expanded in *Phytophthora* genus compared with other oomycetes. Further gain and loss analysis showed that a large number of loss events occurred in *Hyaloperonospora arabidopsidis*, *Pythium ultimum*, and *Albugo laibachii*. In contrast, many duplication events were present in the last common ancestor of the *Phytophthora* species, resulting in expanded LRR-RLKs in *Phytophthora* genomes (Figure S1). Unlike most *A. thaliana* LRR-RLKs harboring more than 10 LRRs, oomycete LRR-RLKs have fewer LRRs varying from 1 to 6, with an average of 3 LRRs (Table S1). However, they shared a relatively conserved LRR motif of LxxLxLxxNxI/L (Figure S2). In addition, a phylogenetic analysis of kinase domains revealed that kinase domains derived from *A. thaliana* LRR-RLKs and metazoan Pelle proteins clustered together, while the KDs of oomycete LRR-RLKs formed a separate clade (Figure S3A). Furthermore, the kinase domains of *P. sojae* LRR-RLKs exhibit conserved features of active protein kinase (Figure S3B). They possess an ATP-binding site and an active site which were generally required for kinase active (Figure S3B). The aforementioned results indicate that oomycete LRR-RLKs exhibit unique structural features, including fewer LRRs and specific kinase motifs, in spite of their overall similarity with plant LRR-RLKs.

Specific *PsRLK* genes affect responses to oomycetecides and bacteria antagonists

CRISPR/Cas9-mediated gene replacement system (Fang and Tyler, 2016) was used to generate knockout mutants for all the 24 *PsRLK* genes (Figure S4A). Knockout lines were screened by genomic DNA PCR (Figure S4B) and verified by sequencing (Figure S4C). Two independent knockout lines were obtained for each *PsRLK*, whereas one line harboring the wild-type *PsRLKs* was recovered from the gene knockout experiment and used as a control strain (CK). We characterized different phenotypes of the CKs, all the knockout mutants and the wild-type strain P6497 but only show the results from one representative knockout line for each *PsRLK* because the two corresponding lines exhibit similar and comparable phenotypes.

None of PsRLK knockout mutants had significant defect in growth rate or hyphae morphology (Table S2). Next, we aimed to investigate whether PsRLKs confer oomycetecide tolerance by testing the sensitivity of all Δ*PsRLK* mutants to metalaxyl (Matson et al., 2015) and fluopicolide (Zhang et al., 2019), both of which are widely used pesticides for *P. sojae* management (Gisi and Sierotzki, 2015). While no mutant exhibited altered fluopicolide tolerance, Δ*PsRLK12/16/20/23* was significantly more sensitive to metalaxyl than the controls and other mutants (Figure S5 and Table S2).

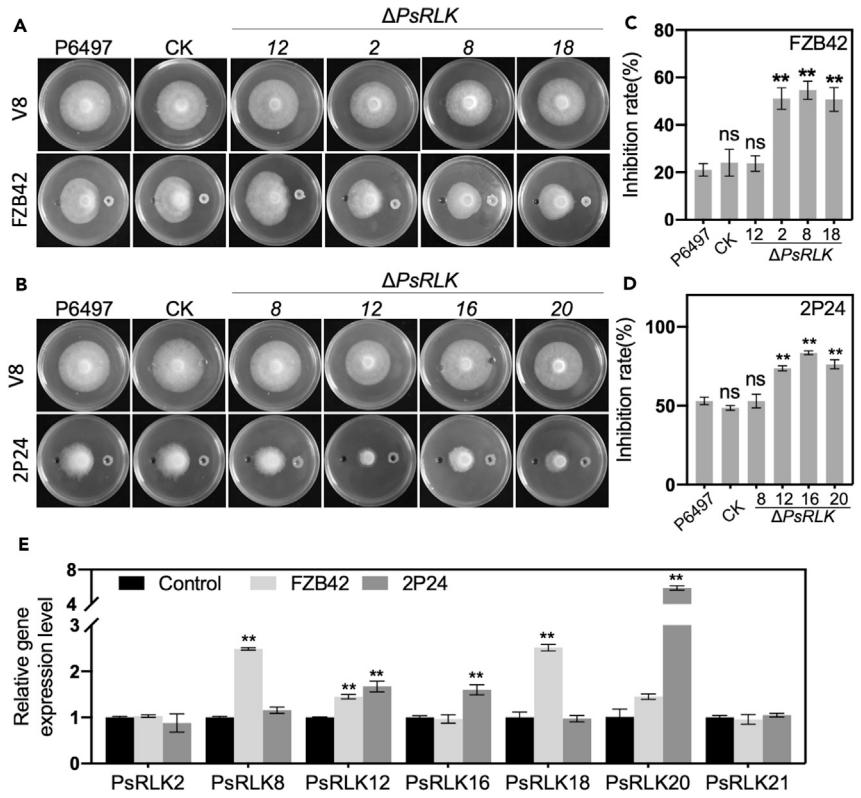

Figure 2. Specific PsRLKs confer tolerance to two bacteria antagonists, FZB42 and 2P24

Wild-type *P. sojae* P6497 was used as the recipient for transgene and two independent knockout mutants were obtained for each *PsRLK* gene (e.g., Δ*PsRLK2* means a transgenic line with *PsRLK2* gene being deleted). CK is a transgenic strain, in which each *PsRLK* gene is intact. The phenotypes of the two mutants and CK for each gene were examined and compared. The photos only show a representative mutant strain for one gene.

(A and B) Inhibition *P. sojae* hyphal growth by *B. amyloliquefaciens* FZB42 (A) and *P. fluorescens* 2P24 (B). All the *PsRLK* knockout strains, together with P6497 and CK, were cultured on V8 medium alone or cocultivated with either FZB42 (A) or 2P24 (B). Photos were taken at 4 dpi and one transgenic strain for each gene mutant was shown because of the comparable and stable phenotypes.

(C and D) Inhibition rates of the indicated strains cocultivated with FZB42 (C) or 2P24 (D). The data were calculated [(colony area on V8 plates alone – colony area on V8 plates with biocontrol bacteria)/colony area on V8 Plates alone] and compared. Colony areas were measured in each independent biological experiment after cultured for 5 days at 25°C. All experiments were repeated at least three times with similar results. The values are means ± SD, n = 10 (ANOVA: **, $P < 0.01$; ns indicates no significant difference).

(E) Relative expression levels of the indicated *PsRLK* genes. *P. sojae* was incubated with control, FZB42, or 2P24 for 2 h and harvested for RNA extraction. Relative expression levels of each gene were normalized with *actin* gene as the internal standard and presented as means ± SD (n = 3, $p < 0.01$, Student's t test). These experiments were repeated three times with similar results.

Utilization of biocontrol bacterial species including *Bacillus* and *Pseudomonas* species is also a promising approach for the control of *Phytophthora* diseases (Gao et al., 2012; Wu et al., 2018). To evaluate the participation of PsRLKs in *P. sojae* response to bacteria antagonists, the confrontation culture method was performed to determine the sensitivity of *P. sojae* Δ*PsRLK* mutants to two biological agents, *Bacillus amyloliquefaciens* FZB42 (Wu et al., 2018) and *Pseudomonas fluorescens* 2P24 (Gao et al., 2012). Compared to P6497 and CK, Δ*PsRLK2/8/18* was more sensitive to FZB42 inhibition (Figures 2A and 2B), whereas Δ*PsRLK12/16/20* formed another group whose growth can be more effectively inhibited by 2P24 (Figures 2C and 2D). To understand the molecular basis for these PsRLK responses to FZB42 or 2P24 during confrontation, we performed transcription analysis of these *PsRLK* genes. Indeed, coculture with FZB42 induced upregulated expression of *PsRLK8/12/18* genes, whereas *PsRLK12/16/20* genes were upregulated when incubated 2P24 (Figure 2E). Thus, we suggest that PsRLKs may play various and essential roles in responses to oomycetecides and bacteria antagonists.

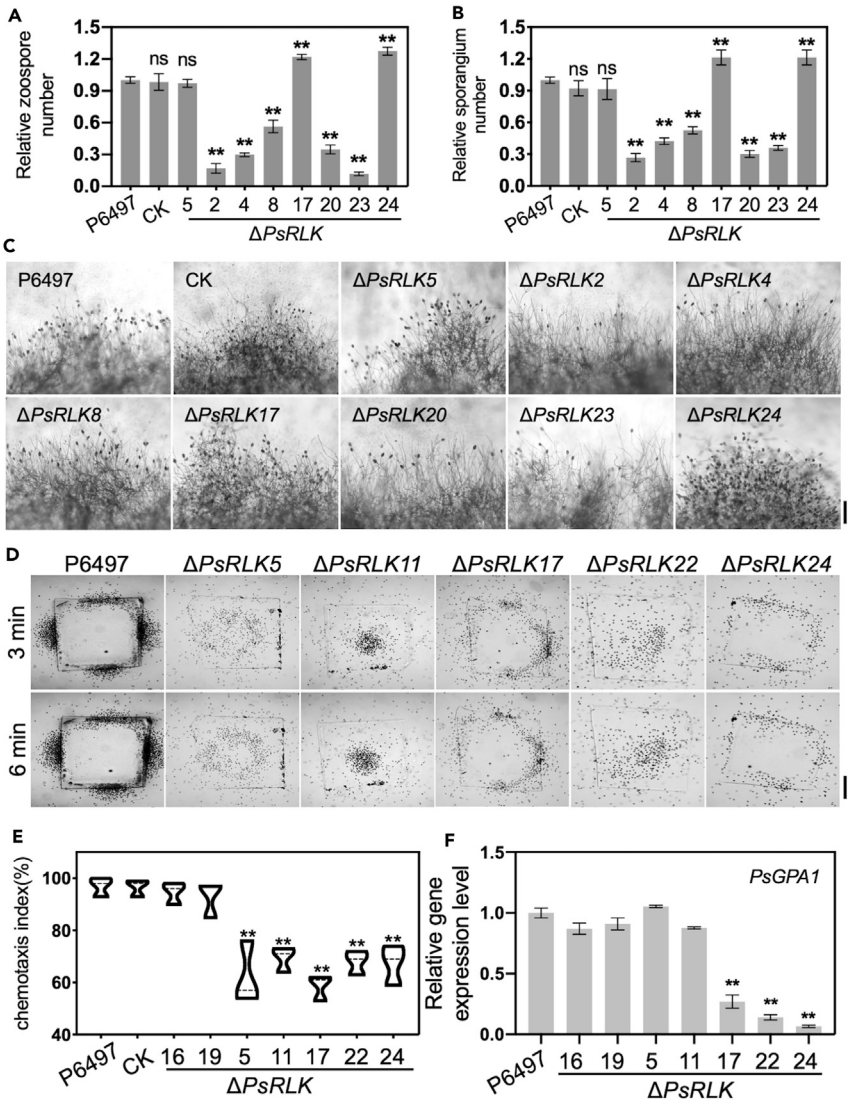

Figure 3. PsRLKs differentially regulate sporangium formation and chemotaxis of *P. sojae* zoospores

(A and B) Relative numbers of zoospores (A) and sporangia (B). P6497 zoospore or sporangia numbers were normalized to 1 and the numbers of all other mutants were calculated accordingly. The values are means ± SD, n = 6 (ANOVA: **, $P < 0.01$; ns indicates no significant difference).

(C) Microscopic visualization of sporangium production. The indicated strains were examined under a microscope at 4× magnification. Scale bar = 50 μm.

(D) *P. sojae* chemotaxis assay to isoflavones. Agarose plugs containing 15 μM isoflavones were placed in microscopic chambers and filled with equal amounts of zoospores. Photographs were taken at 3 and 6 min of incubation. The typical photos were shown. Scale bar = 50 μm.

(E) Comparison of chemotropic indexes. The chemotropic index was calculated as (Σtotal − Σsolv)/Σtotal × 100. The values are means ± SD (n = 3). Each index data point includes at least three biological replicates (ANOVA: **, $P < 0.01$). Σ_{total} is the number of total zoospores and Σsolv is the number of zoospores that swim toward the solvent DMSO side.

(F) Relative expression levels of *PsGPA1* gene in the indicated mutants. *PsGPA1* expression in P6497 was set as the control. *P. sojae actin* gene was used as the reference. The values are means ± SD, n = 3. All qRT-PCR experiments have three biological replicates (ANOVA: **, $P < 0.01$).

PsRLK2/4/8/17/20/23/24 promote zoospore production

To investigate the contribution of individual PsRLK on zoosporogenesis, we tested the zoospore production of all the mutants. Five *PsRLK* genes mutants (Δ*PsRLK2/4/8/20/23*) produced fewer zoospores (Figure 3A) and exhibited lower sporangia density (Figure 3B), whereas higher numbers of zoospores and

sporangia were observed in Δ*PsRLK17* and Δ*PsRLK24* when compared with CK, P6497, and the other mutants. Zoospore productions reduced most severely in Δ*PsRLK2* (−82.6%) and Δ*PsRLK23* (−86.4%). Δ*PsRLK2* also showed more than 70% reduction of sporangia number. Meanwhile, the sporangia production of Δ*PsRLK17* and Δ*PsRLK24* was increased by 21.3% and 30.8%, respectively. Despite that zoospore and sporangia productions varied in these mutants, they showed no visible morphology changes across all the wild-type and mutant strains (Figure 3C). Thus, PsRLK2/4/8/17/20/23/24 would appear to have the specific quantity-regulation roles in sporangium formation and zoospore production.

PsRLK5/11/17/22/24 are involved in the chemotaxis response of zoospores

The chemotaxis of *P. sojae* zoospores to isoflavones is critical for recognizing host and initiating infection in the disease cycle (Hua et al., 2008; Morris et al., 1998). Zoospore chemotaxis of the *PsRLK* knockout mutants were tested using the isoflavone as described previously (Hua et al., 2008; Zhang et al., 2016). In this assay, the wild-type P6497 zoospores reached the agarose plug containing 15 μM isoflavone and began to encyst within 3 min (Figure 3D). In contrast, most zoospores of Δ*PsRLK5/11/17/22/24* mutants swam around the agarose plug and the encystment was not observed even after 6 min (Figure 3D). The results suggest that disrupting any of the above five *PsRLKs* could impair zoospore chemotaxis response. To verify the observation, we designed another chemotaxis assay with its model being showed in Figure S6A and found that all P6497 zoospores reached the isoflavone side in 5 min, whereas moiety zoospores of the five gene knockout mutants swam toward the side away from isoflavones (Figure S6B). Chemotaxis indexes were calculated by counting the distribution of zoospores in the chamber. Δ*PsRLK5/11/17/22/24* all showed about 30% reduction in chemotaxis indexes when compared with the controls (Figure 3E).

Furthermore, to determine the effect of these five PsRLK genes on virulence, the zoospores of Δ*PsRLK5/11/17/22/24* were inoculated onto the hypocotyls of the etiolated soybean seedlings. The results showed no obvious difference in the spread of disease symptoms among P6497 and the mutants (Figures S7A and S7C). In contrast, in the soybean root-dipping inoculation assay with zoospores suspension of these mutants, smaller lesion was observed in the soybean inoculated with Δ*PsRLK5/11/17/22/24* zoospores compared with P6497 (Figures S7B and S7D). Thus, the results demonstrate that these genes are not directly related to virulence but are critical for recognizing host chemotaxis signals.

As *P. sojae* chemotaxis to soybean isoflavones is regulated by G-protein α subunit PsGPA1-mediated signaling (Hua et al., 2008; Latijnhouwers et al., 2004), we tested whether PsRLK5/11/17/22/24 regulate zoospore chemotaxis via modulating *PsGPA1* expression by measuring transcript accumulations of *PsGPA1* in Δ*PsRLK5/11/17/22/24* zoospores. Compared to Δ*PsRLK16/19* and P6497, Δ*PsRLK17/22/24* but not Δ*PsRLK5/11* exhibited significantly downregulated *PsGPA1* expression (Figure 3F). These results suggest that *PsRLK17/22/24* may affect chemotaxis sensing of isoflavones via promoting *PsGPA1* expression.

PsRLK5/11/17/22/24 physically interact with G-protein α subunit PsGPA1

Considering that G-protein subunits physically interact with LRR-RLKs, such as FLS2 and BAK1, to mediate downstream signaling pathways in *Arabidopsis* (Liang et al., 2016; Peng et al., 2018), we hypothesized that PsRLKs and PsGPA1 could form protein complex to regulate chemotaxis and found that all five chemotaxis-related PsRLKs (5/11/17/22/24) showed physical interactions with PsGPA1 in a luciferase (Luc) complementation imaging (LCI) assay conducted on *Nicotiana benthamiana* leaves (Figure 4A). PsRLK-PsGPA1 interaction brought N-(NLuc) and C-(CLuc) terminal fragments of Luc together and restored its activity (Chen et al., 2008). As negative controls, empty vector (EV), PsRLK15 and PsRLK19 did not generate any interaction signal with PsGPA1 (Figure 4A), and the known interaction between FLS2 and Arabidopsis G-protein XLG2 was used as a positive control (Figure 4A). To determine whether individual PsRLK interacts with PsGPA1 via its KD (PsRLK^{KD}), we generated the truncated intracellular PsRLK^{KD} and found that PsRLK5/11/17/22/24^{KD} all retained the PsGPA1-interacting capacities of their full-length proteins (Figure 4B). Furthermore, all five PsRLK^{KD}-PsGPA1 interactions were successfully verified by both yeast two-hybrid (Y2H) (Figure 4C) and pull-down (Figure 4D) assays using PsRLK15^{KD} as a negative control. The KD of PsRLKs exhibits conserved features of active protein kinases (Figure S3B). An *in vitro* kinase reaction assay revealed that PsRLK5/11/17/22/24^{KD} all showed strong autophosphorylation activity (Figure S8). Collectively, PsRLK5/11/17/22/24 would appear to regulate G protein in a kinase-dependent manner.

PsRLK8/12/15/18/19/20 is a positive regulator of *P. sojae* virulence

In a *P. sojae* zoospore inoculation assay using soybean seedlings as the host, six gene knockout mutants (Δ*PsRLK8/12/15/18/19/20*) exhibited significant fewer necrotic lesions at 48 hpi when compared with

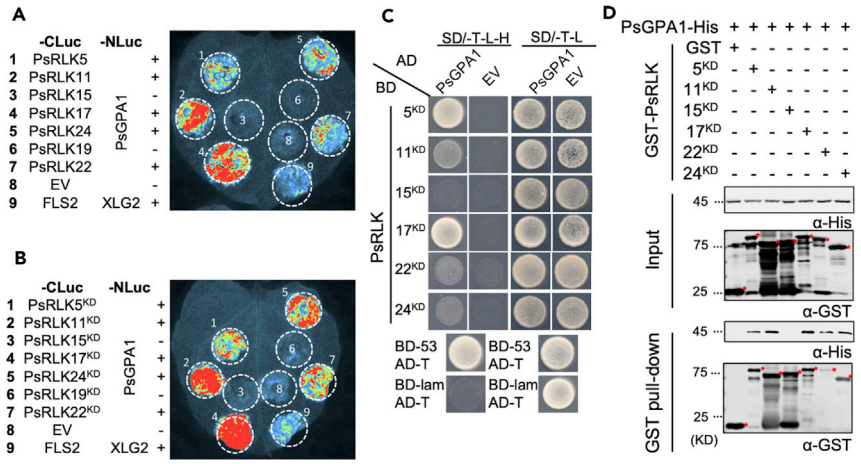

Figure 4. PsRLKs physically interact with PsGPA1 via their KDs

(A and B) Interactions of PsGPA1 with the indicated PsRLK (A) or PsRLK^{KD} (B) revealed by the LCI assay in *N. benthamiana* leaves. Images show luminescence signals under a CCD camera. Combination of FLS2-NLuc and XLG2-CLuc was used as a positive control. EV represents the empty vector control.

(C) Interactions between the indicated PsRLK KDs and PsGPA1 in the yeast two-hybrid (Y2H) assay, DNA sequence encoding each individual PsRLK^{KD} was cloned into the bait vector pGBKT7 (BD). *PsGPA1* was cloned into the prey vector pGADT7 (AD). Combination of BD-53 and AD-T was used as a positive control. Combination of BD-Lam and AD-T was used as a negative control. Yeast transformants were grown on SD/-Trp/-Leu (SD/-T-L) and selected on SD/-Trp/-Leu/-His/(SD/-T-L-H). The plates were photographed 2 days after inoculation.

(D) PsGPA1 physically interacts with five PsRLK^{KD}s *in vitro*. Each GST-PsRLK^{KD} or GST bound resins was incubated with *E. coli* supernatant containing PsGPA1-His. Protein bands of GST- PsRLK^{KD} are marked by asterisks. The presence of His-tagged proteins was detected by Western blot using the anti-His tag antibody.

P6497, the CKs, and other mutants (Figure 5A). As a consequence, all six gene mutations caused more than 50% reductions of relative *P. sojae* biomass in infected soybean seedlings (Figure 5B), with about 90% reductions observed for Δ*PsRLK8* and *20* (Figure 5B).

DAB staining revealed that 60%–80% of the soybean epidermal cells infected by Δ*PsRLK8/18/19/20* exhibited much stronger H_2O_2 levels than those of the two control lines P6497 and Δ*PsRLK4*, a mutant with normal virulence (Figures 5C and 5D), suggesting that the four mutation lines partially lost the ability to interfere with host H_2O_2 accumulation at the infected sites. Interestingly, enhanced H_2O_2 levels were not detected in cells infected with Δ*PsRLK12/15* (Figures 5C and 5D), other two lines with the reduced virulence (Figures 5A and 5B). Consistent with virulence measurement and DAB staining of H_2O_2 accumulation results, Δ*PsRLK8/18/19/20* all exhibited significantly increased sensitivity to H_2O_2 when compared with P6497 (Figures 5E and 5F). No changes of H_2O_2 sensitivity were observed for Δ*PsRLK12* or *15* (Figures 5E and 5F), which is consistent with their irrelevance to H_2O_2 accumulation (Figures 5C and 5D). These results together indicate that PsRLK8/18/19/20 and PsRLK12/15 promote *P. sojae* virulence dependent and independent of oxidative stress, respectively.

Strikingly, Δ*PsRLK4* was more sensitive to H_2O_2 but did not show any significant impact on virulence or soybean H_2O_2 accumulation (Figure 5), which suggested that PsRLK4 may be involved in a distinct pathway that is regulated by oxidative stress, irrelevant to virulence, but have no feedback effect on H_2O_2 accumulation.

PsRLKs forms a protein interaction network

To generate the interaction network of PsRLKs that potentially form homo- and hetero-oligomeric complexes, we performed the LCI assay, by which each PsRLK was fused with Nluc or CLuc fragment at C-terminal and expressed in *N. benthamiana* (Figure 6A). First, PsRLK8 was selected to validate the feasibility of the assay, and the results clearly showed that it may associate with PsRLK10/12/14/17/20/21, as well as itself, but not all other PsRLKs (Figures 6B, 6C, and S7). Among six genes related to virulence (Figures 5A and 5B), PsRLK8 interact with PsRLK12 and PsRLK20 but not with PsRLK15/18/19 (Figure 6B). The results suggest that PsRLK8 may regulate virulence via forming homodimer, heterodimers, and/or higher-order complexes.

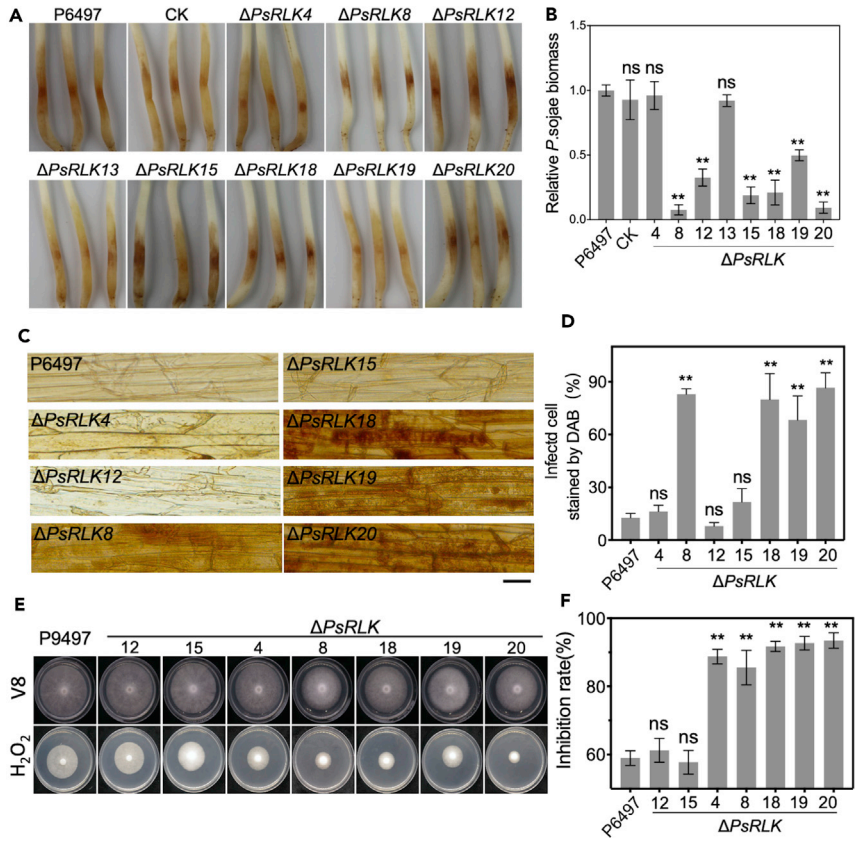

Figure 5. Six PsRLKs are required for *P. sojae* virulence

(A) Lesions on the etiolated hypocotyls of soybean (cultivar Hefeng 35) infected with the zoospores of the indicated strains. The photographs were taken at 48 hpi and the experiments were repeated at least three times with similar results.

(B) The relative biomass of *P. sojae* in the inoculated etiolated hypocotyls. Each sample was harvested at 48 hpi for qRT-PCR. Relative ratios of *P. sojae*/soybean DNA were calculated. The values are means ± SD of three independent biological replicates (ANOVA: **, $P < 0.01$; ns indicates no significant difference).

(C) DAB staining of the infected areas. The representative images were taken at 36 hpi (Scale bar, 10 μm).

(D) The infected cells straining by DAB were counted 36 hpi after inoculation. The values are means ± SD, n = 3 (ANOVA: **, $P < 0.01$; ns indicates no significant difference).

(E) H_2O_2 sensitivity assay. The indicated strains were cultured in V8 without (upper panel) or with (lower panel) 6 mM H_2O_2. The photos were taken at 5 days after treatment.

(F) The inhibition rate of H_2O_2. The inhibition rate (%) of each strain was calculated [(growth rate on V8 plates without H_2O_2 – growth rate on V8 plates with H_2O_2)/growth rate on V8 Plates without H_2O_2] and compared. The values are means ± SD, n = 3 (ANOVA: **, $P < 0.01$; ns indicates no significant difference).

Next, we tested 576 PsRLK pairs and found 64 positive interactions (Figures 6C and S9). No interaction was detected for PsRLK2/6/7/9/11/13/15/19/22/23/24, among which, seven genes were shown to regulate zoospore production, chemotaxis, or virulence (Figures 1, 2, and 3). PsRLK1/8/10/14/17/21 exhibited self-interactions. As three major nodes, PsRLK10, PsRLK14, and PsRLK21 had 11, 9, and 9 interacting PsRLK partners, respectively. Eleven candidates, including PsRLK2/6/7/11/13/15/19/20/22/23/24, could not form RLK complex in this assay. And, at least 4 interactors were detected for PsRLK1/4/8/17/18. As no visible phenotype was detected for Δ*PsRLK1/3/6/7/9/10/13/14/16/21* in this study, some of them may have functional redundancy, which is common for *Arabidopsis* LRR-RLKs (He et al., 2018).

PsRLK21 and PsRLK10/17 jointly regulate virulence via direct interactions

As PsRLK21 is an important interaction node and none phenotype alteration was found in its deletion mutant, we generated two independent double-knockout mutants (Δ*PsRLK17&21* and Δ*PsRLK10&21*). No visible defect in vegetative growth or morphology was observed in either mutant (Figure S10A). In the zoospore inoculation assay using the etiolated soybean seedlings, both Δ*PsRLK17&21* and Δ*PsRLK10&21*

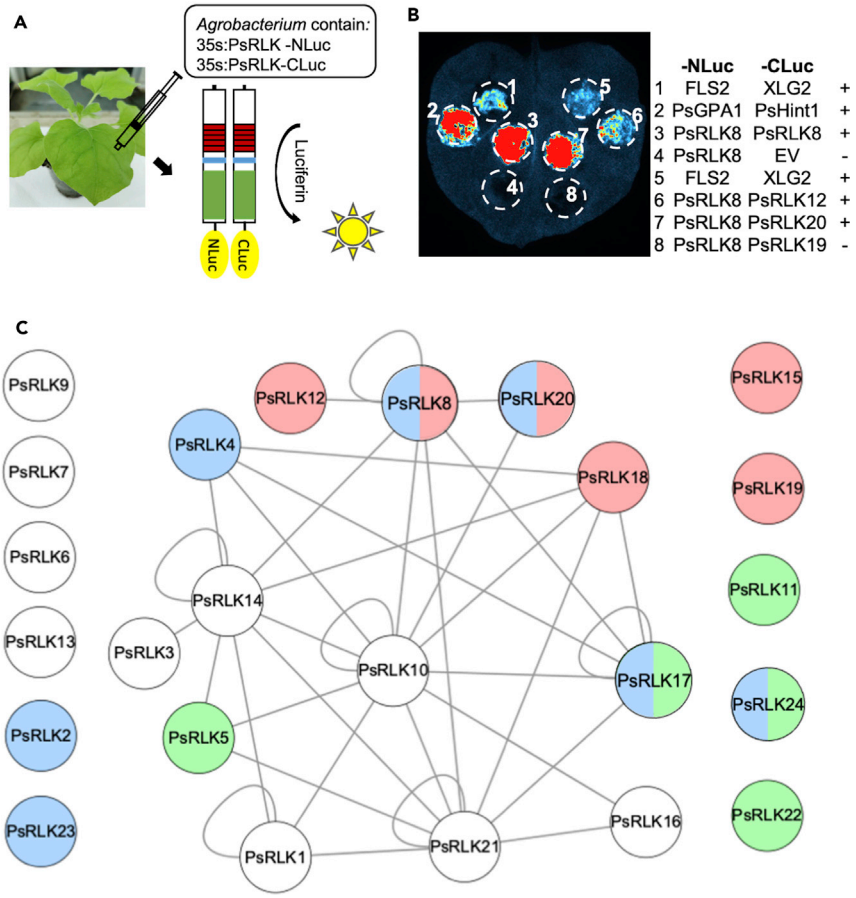

Figure 6. PsRLK interactome in *P. sojae*

(A) The sketch map of LCI assay in plants.

(B) Interaction of PsRLK8 with PsRLK8/12/20 in *N. benthamiana* leaves. The indicated constructs were transiently expressed in *N. benthamiana* plants for luciferase complementation assay. Two combinations of FLS2-Nluc with XLG2-Cluc and PsGPA1-Nluc with PsHint1 were used positive controls. Combination of PsRLK8-Nluc and EV-Cluc was used as negative control.

(C) The PsRLK interaction network. Nodes in green, pale red, and yellow represent indicated PsRLK functions in zoospores chemotaxis, virulence and zoospore production, respectively. The network was visualized using Cytoscape 3.6.1.

See also Figure S9.

caused much smaller lesion sizes at 48 hpi when compare with P6497 and three single mutant controls of Δ*PsRLK21*, Δ*PsRLK17*, and Δ*PsRLK10* (Figure 7A). Consistently, *P. sojae* biomass accumulations of both double mutants were significantly reduced in inoculated soybean hypocotyls (Figure 7B). They also showed increased sensitivity to H_2O_2 (Figure S11) as well as reduced ability to interfere with host H_2O_2 accumulation at the infected sites (Figure 7C). The two double mutants behaved differently in zoospore and sporangia production. Compared with P6497, Δ*PsRLK21, and* Δ*PsRLK10,* significant reductions (more than 50%) of zoospore and sporangia numbers were observed in the double mutant, Δ*PsRLK10&21*. However, Δ*PsRLK17&21* exhibited ~21% increase in zoospores and sporangia numbers, but no significant difference was observed between Δ*PsRLK17&21* and Δ*PsRLK17* (Figures S10B–10D). Collectively, these results implied that PsRLK21 and PsRLK10/17 may jointly regulate virulence by direct interaction.

To confirm interaction between PsRLK21 and PsRLK10/17, we first generated two truncated mutants of PsRLK21, the N-terminal ECD (PsRLK21^{ECD}) and the intracellular KD (PSRLK21^{KD}). In the LCI assay, PsRLK21^{ECD}, as well as the full length, but not PSRLK21^{KD}, could interact with PsRLK10/17 (Figure 7D). Furthermore, ECD-mediated PsRLK21 and PsRLK10/17 interaction was validated in a GFP coimmunoprecipitation (Co-IP) assay (Figure 7E) in which PsRLK21^{ECD}-FLAG was transiently coexpressed with PsRLK10^{ECD}-GFP or PsRLK17^{ECD}-GFP in *N. benthamiana*.

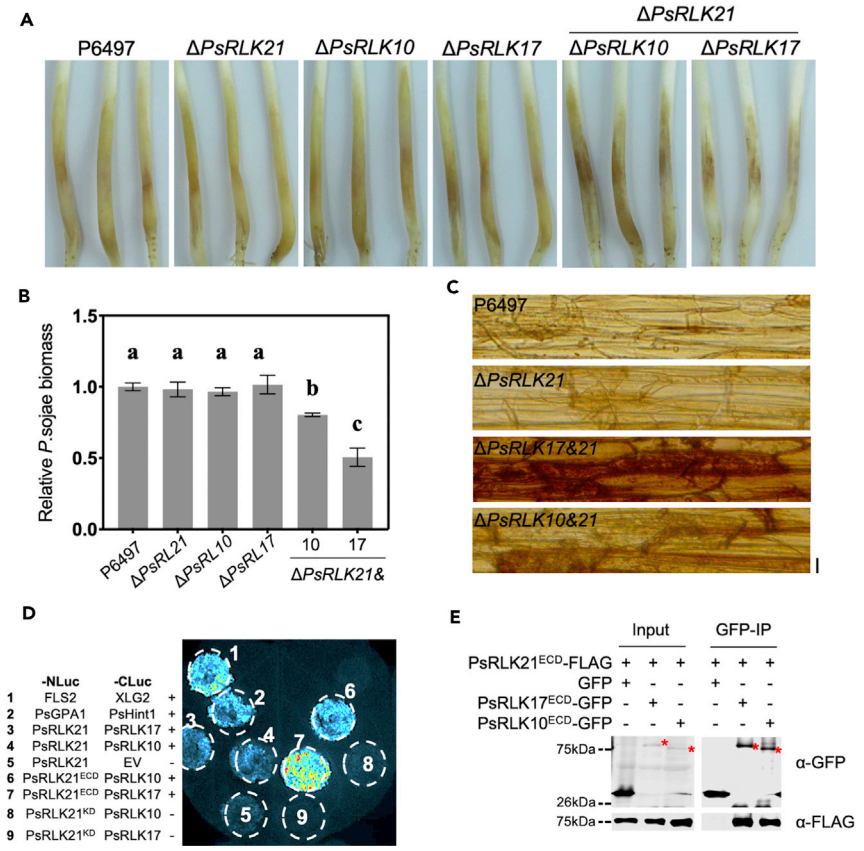

Figure 7. PsRLK21 and PsRLK10/17 jointly regulate *P. sojae* virulence via direct interactions

(A) Two double-knockout mutants (Δ*PsRLK21&17* and Δ*PsRLK21&10*) exhibited reduced virulence. Soybean hypocotyls were inoculated with equal amounts of zoospores from the indicated strains. Photos were taken at 48 hpi.

(B) The relative biomass of *P. sojae* in the inoculated hypocotyls. The indicated samples were harvested at 48 hpi for qRT-PCR. Ratios of *P. sojae*/soybean DNA were calculated. Error bars represent standard deviation of the mean (n = 5). Different letters indicate significant differences based on ANOVA analysis ($P < 0.05$).

(C) DAB staining of the infected areas. Representative images were graphed at 36 hpi (Scale bar, 10μm).

(D) LCI assay in *N. benthamiana* leaves. NLuc-fused PsRLK21^{ECD} was coexpressed with either PsRLK10 or PsRLK17 fused with CLuc. Two combinations of FLS2-Nluc with XLG2-Cluc and PsGPA1-Nluc with PsHint1 were used as positive controls. Combination of PsRLK21-Nluc and EV-Cluc was used as a negative control. Images were taken 2 days after infiltration.

(E) Co-IP assay in *N. benthamiana* leaves. PsRLK20^{ECD}-FLAG was coexpressed with PsRLK10-GFP or PsRLK17-GFP Protein bands were detected by Western blot with anti-FLAG or anti-GFP antibodies.

DISCUSSION

LRR-RLKs, a large family of sensory proteins well-documented in plants, have been bioinformatically identified in several eukaryotes including oomycetes (Diévart et al., 2011). However, the functions of nonplant LRR-RLKs are still unknown. In this study, all the 24 *P. sojae* LRR-RLK encoding genes were functionally analyzed using gene deletion approach. In summary, 15 PsRLKs genes have diverse functions in zoospore development and chemotaxis, virulence and metalaxyl sensitivity, as well as response to bacteria antagonists. Five PsRLKs regulate zoospore chemotaxis by direct interacting with G-protein α subunit PsGPA1, an important regulator of *P. sojae* zoospore motility and chemotaxis. Multiple PsRLKs form a network of homointeractions and heterointeractions that involved in various regulation process. Using PsRLK21 as an example, we demonstrate that the functional redundancy may exist. For example, PsRLK21 and PsRLK10/17 jointly regulate virulence via direct interactions. Our findings highlight the extensive roles of LRR-RLKs in oomycete asexual development, pathogenesis, and stress responses.

Earlier studies established the existence of LRR-RLKs in oomycetes and the correlation between their differential expression and the infection process (Diévart et al., 2011). However, there has been no systematic

exploration of *Phytophthora* LRR-RLK families. Here, we searched candidate LRR-RLK genes in *P. sojae* genome by using the known reference sequences from plants. An LRR-RLK family has been identified in *P. sojae*, with all members exhibiting a typical structure of LRR-containing ECD, TM and KD (Magalhaes et al., 2016; Man et al., 2020). Our phylogenetic and functional analyses of PsRLKs demonstrate that *Phytophthora* and plant LRR-RLKs evolve independently and may have distinct biological functions. In our comparative analysis of *P. sojae* and *Arabidopsis* LRR-RLKs, the amino acid sequences of their LRR motifs are conserved, but PsRLKs generally have much fewer LRRs, which may be relevant to the differential signals perceived by oomycete and plant LRR-RLKs. Interestingly, the serine/threonine KDs of oomycete LRR-RLKs is independent to *A. thaliana* LRR-RLKs and metazoan pelle proteins. The relatively low similarities shared by *P. sojae* and *Arabidopsis* KDs may reflect the differences of their downstream phosphorylating targets. Considering the major roles of LRR-RLKs in plant life cycle and plant-environment interaction, the PsRLKs may play a key role in *Phytophthora* life cycle. Furthermore, the large numbers of LRR-RLKs evolved in plants may at least partially offset their lack of G-protein-coupled receptors (GPCRs), which represent the largest group of transmembrane proteins found in animals and fungi (El-Defrawy and Hesham, 2020). Interestingly, oomycetes harbor both LRR-RLKs and GPCRs, which makes them unique in the species evolution theme.

There are more than 200 LRR-RLKs in *Arabidopsis* (Shiu and Bleecker, 2001a). They function as receptors for phytohormones, endogenous peptides, and pathogen-derived molecules and thereby regulate plant growth, development, and defense responses (Couto and Zipfel, 2016; Tang et al., 2017). As a soybean pathogen, *P. sojae* evolves LRR-RLKs to mainly facilitate its development and infection process. Currently, numerous management strategies are applied to control the *Phytophthora* disease during agricultural production. Metalaxyl, a phenyl amide fungicide, is the main oomyceticide and the most viable means for the management of *P. sojae* (Gisi and Sierotzki, 2015; Matson et al., 2015). Previous studies have revealed that metalaxyl inhibits the synthesis of ribosomal RNA, suggesting that it may target RNA polymerase I in *P. infestans* (Chen et al., 2018). To date, several studies has shown an assay based on RPA190 will not be sufficient to mediate the sensitivity levels of *Phytophthora* resistance isolates (Matson et al., 2015; Wang et al., 2021) and other genes may contribute to stable metalaxyl resistance. In this study, we observed that the mutants of four *PsRLK* genes (ΔPsRLK12/16/20/23) increased sensitivity to metalaxyl but not fluopicolide (Figure S4). Thus, these four PsRLKs may serve as positive regulators mediating metalaxyl sensitivity. Interestingly, no mutual interaction was observed among these four PsRLKs (Figure 6). Further work should focus on deciphering the molecular mechanisms of these four PsRLKs in metalaxyl resistance to reveal new targets to combat oomycete pathogens.

Owing to environmentally friendly characteristics, biocontrol has received great attentions. Several bacterial antagonists have been discovered with anti-*Phytophthora* effects, and antibiosis of bacteria has also been widely studied during bacteria and filamentous pathogen interaction (BFI) (De Vrieze et al., 2018; Syed-Ab-Rahman et al., 2018; Vrieze et al., 2019; Wagner et al., 2018). Recently, *Phytophthora* pathogens were found to deploy effector proteins to directly interfere with bacterial growth and motility to block contact of bacterial (Wang et al., 2020). *Verticillium dahliae*, a soil-borne fungus, uses VdAMP2 effector proteins to modulate microbiome compositions inside and outside the host (Snelders et al., 2020, p.). The transcriptomic analyses of BFI demonstrated that the pathogens may react to the presence of the partner microorganisms and respond differentially depending on the interacting partners (Deveau et al., 2018; Tomada et al., 2017). However, little is known about the ability and mechanism of pathogens to perceive and recognize the environmental microorganisms. Here, the mutants of Δ*PsRLK12/16/19* were highly sensitive to *Pseudomonas* strain 2P24, whereas other three mutants (Δ*PsRLK2/8/18*) were less resistance to *B. amyloliquefaciens* strain FZB42 (Figure 2), some of whose encoding genes were specifically up-regulated by FZB42 and 2P24. It has been proposed that filamentous pathogens have evolved a sophisticated innate immune system and receptors to recognize and defense bacteria (Deveau et al., 2018). Our study suggests that *P. sojae* RLKs may play important roles in its innate immune system to combat with bacterial antagonists, which is reminiscent to plant RLKs during interaction with pathogens.

P. sojae uses elaborate mechanisms to overcome plant innate immune system for successful infection (Chepsergon et al., 2020). In this research, we demonstrate that PsRLKs play diverse roles in *P. sojae* sporangia and zoospore production, chemotaxis response, suppression of host H_2O_2 accumulation and virulence. Zoospore releasing from sporangia could swim to soybean root to initialize infection, which depends on chemotaxis (Judelson and Blanco, 2005). Recent studies have shown that the sole G protein α subunit *PsGPA1* is involved in zoospore chemotaxis and acts as a negative regulator of sporangium production in *P. sojae* (Hua et al., 2008; Qiu et al., 2020). Here, we show that five PsRLKs (5/11/17/21/24) interact with PsGPA1 via their KDs, which is the first report that the Gα subunit interacts directly with LRR-RLKs in the oomycete. The interactions may lead

to the modifications of PsGPA1, such as phosphorylation. It is reasonable to infer that PsRLKs and the G protein regulate zoospore production and chemotaxis through unknown downstream factors.

Four PsRLKs (8/18/19/20) positively regulate *P. sojae* virulence via suppressing H_2O_2 accumulation at the infection site. ROS production functions as a second messenger to induce various plant defense responses and is essential for pathogen-associated-molecular-pattern-triggered immunity (Dou and Zhou, 2012). During *Phytophthora*-host interactions, plant ROS production can be regulated by RXLR effectors (Dong et al., 2011; Li et al., 2019) and other *Phytophthora* secreted proteins including elicitins, crinkling- and necrosis-inducing proteins, and necrosis- and ethylene-inducing-like proteins (Li et al., 2016; Ma et al., 2015). It will be interesting to investigate the potential connections between PsRLKs and these effector proteins and the host signals that could be perceived by *P. sojae*.

Mitogen-activated protein kinase (MAPK) cascades function as key signal transducers downstream of RLKs to involved in various signal pathways in plants (Zhang et al., 2018; Zhou and Zhang, 2020). In *P. sojae*, three MAPKs named PsMPK1, PsMPK3 (PsSAK1), and PsMPK7 are essential for spore development, osmotic and oxidative stresses responses, and pathogenicity (Gao et al., 2015; Li et al, 2010, 2014). Whether or how PsRLKs modulate MAPK cascades is still unknown. PsMPK7 can be a candidate for connecting PsRLKs and secreted effectors/proteins that regulate ROS production. The mutants that we have generated can facilitate exploration of upstream activators and downstream effectors of PsMPKs, and explain how they function in the MAPK signal transduction pathway.

In plants, ligand perception by LRR-RLK requires coreceptors (Tang et al., 2017; Zhou and Zhang, 2020). For example, interaction between FLS2 and BAK1 is induced by flg22 and subject to extensive regulations by several accessory LRR-RLKs carrying short LRR domains. Systematic study on *Arabidopsis* LRR-RLKs uncovers a comprehensive cell-surface interaction network (CSI^{LRR}) in which LRR-RLKs are connected through interacting with short LRR-RLK hubs (Smakowska-Luzan et al., 2018). In this research, we reveal a PsRLK interaction network with 34 interacting pairs (Figure 6C). Three virulence-related PsRLKs (PsRLK8/12/20) and two zoosporangia-related PsRLKs (PsRLK4/17) form a complex respectively that suggest PsRLKs may coregulate downstream signaling processes via physical interactions among the PsRLK interactome. Likewise, the knockout mutants of six PsRLKs in the PsRLK interactome were detected no difference in our phenotypic assay that implies functional redundancy among PsRLKs. The functional redundancy of LRR-RLK family members adds to the complexity of the signaling network in plants (Albrecht et al., 2008; Zhou and Zhang, 2020). PsRLK functional redundancy is demonstrated in our study using the joint virulence regulation by PsRLK21 and PsRLK10/17 as two examples. We also reveal that PsRLKs interact with each other via their ECDs, which is reasonable as TM is embedded in the plasma membrane and KD is used to interact with and phosphorylate downstream target proteins. Thus, the PsRLKs may act together or redundantly with other membrane proteins to possess a complex signal transduction. Understanding how the other receptor-related genes are being recruited within the PsRLK networks will help to understand how specificity of signaling using LRR-RLKs is being established in *P. sojae*.

In conclusion, an LRR-RLK family with 24 members was systematically characterized in *Phytophthora sojae*, a model species of oomycete. Our results indicate that different *PsRLK* genes play diverse roles in development, virulence, and stress response. Some members could couple with G protein to mediate chemotaxis signaling through their KD domains, whereas some others could form a member protein complex to jointly regulate interaction between *P. sojae* and soybean. Further investigation of the downstream regulate factors of PsRLK network and identify the plant factor or ligands recognized directly or indirectly by different PsRLKs is warranted to elucidate the dynamic and multiple networks of LRR-RLK family in *P. sojae*.

Limitations of the study

Although this study provide evidence showing functional diversification of PsRLKs in sporangia formation, zoospores chemotaxis, pathogenicity, and stress responses, further investigation is needed to fully understand the mechanism of the proposed function of PsRLKs. Specifically, this work has not uncovered the ligands of PsRLKs. Furthermore, approaches of proteomics analysis of PsGPA1 would unravel the interaction model between PsRLK and Gprotein. As described in the discussion section, further research is needed to elucidate the relation between PsRLK-G protein complex and the regulation of chemotaxis of zoospore in *P. sojae*.

STAR★METHODS

Detailed methods are provided in the online version of this paper and include the following:

SUPPLEMENTAL INFORMATION

Supplemental information can be found online at https://doi.org/10.1016/j.isci.2021.102725.

ACKNOWLEDGMENTS

The work was supported by the National Natural Science Foundation of China (31625023, 31721004 and 32072507) and the Fundamental Research Funds for the Central Universities (KYT202001 and JCQY202101).

AUTHOR CONTRIBUTIONS

D.D. conceived the research. J.S., X.L., and D.D. designed research. D.S. completed the bioinformatics analyses. J.S., Y.P., P.J., R.X., and X.X. performed the experiments. D.D., H.P., and J.S. wrote the manuscript. All authors read and approved the final manuscript.

DECLARATION OF INTERESTS

The authors declare no competing interests.

Received: January 14, 2021
Revised: May 1, 2021
Accepted: June 11, 2021
Published: July 23, 2021

REFERENCES

Albrecht, C., Russinova, E., Kemmerling, B., Kwaaitaal, M., and de Vries, S.C. (2008). *Arabidopsis* SOMATIC EMBRYOGENESIS RECEPTOR KINASE proteins serve brassinosteroid-dependent and -independent signaling pathways. Plant Physiol. *148*, 611–619. https://doi.org/10.1104/pp.108.123216.

Chen, F., Zhou, Q., Xi, J., Li, D., Schnabel, G., and Zhan, J. (2018). Analysis of RPA190 revealed multiple positively selected mutations associated with metalaxyl resistance in *Phytophthora infestans*: metalaxyl resistance in *Phytophthora infestans*. Pest Manag. Sci. *74*, 1916–1924. https://doi.org/10.1002/ps.4893.

Chen, H., Zou, Y., Shang, Y., Lin, H., Wang, Y., Cai, R., Tang, X., and Zhou, J.M. (2008). Firefly luciferase complementation imaging assay for protein-protein interactions in plants. Plant Physiol. *146*, 368–376. https://doi.org/10.1104/pp.107.111740.

Chepsergon, J., Motaung, T.E., Bellieny-Rabelo, D., and Moleleki, L.N. (2020). Organize, don't agonize: strategic success of *Phytophthora* species. Microorganisms *8*, 917. https://doi.org/10.3390/microorganisms8060917.

Chinchilla, D., Shan, L., He, P., de Vries, S., and Kemmerling, B. (2009). One for all: the receptor-associated kinase BAK1. Trends Plant Sci. *14*, 535–541. https://doi.org/10.1016/j.tplants.2009.08.002.

Chinchilla, D., Zipfel, C., Robatzek, S., Kemmerling, B., Nürnberger, T., Jones, J.D., Felix, G., and Boller, T. (2007). A flagellin-induced complex of the receptor FLS2 and BAK1 initiates plant defence. Nature *448*, 497–500.

Cohen, Y., and Coffey, M.D. (1986). Systemic fungicides and the control of oomycetes. Annu. Rev. Phytopathol. *24*, 311–338. https://doi.org/10.1146/annurev.py.24.090186.001523.

Couto, D., and Zipfel, C. (2016). Regulation of pattern recognition receptor signalling in plants.

Nat. Rev. Immunol. *16*, 537–552. https://doi.org/10.1038/nri.2016.77.

De Vrieze, M., Germanier, F., Vuille, N., and Weisskopf, L. (2018). Combining different potato-associated *Pseudomonas* strains for improved biocontrol of *Phytophthora infestans*. Front. Microbiol. *9*, 2573. https://doi.org/10.3389/fmicb.2018.02573.

Deveau, A., Bonito, G., Uehling, J., Paoletti, M., Becker, M., Bindschedler, S., Hacquard, S., Hervé, V., Labbé, J., Lastovetsky, O.A., et al. (2018). Bacterial–fungal interactions: ecology, mechanisms and challenges. FEMS Microbiol. Rev. *42*, 335–352. https://doi.org/10.1093/femsre/fuy008.

Diévart, A., and Clark, S.E. (2003). Using mutant alleles to determine the structure and function of leucine-rich repeat receptor-like kinases. Curr. Opin. Plant Biol. *6*, 507–516. https://doi.org/10.1016/S1369-5266(03)00089-X.

Diévart, A., Gilbert, N., Droc, G., Attard, A., Gourgues, M., Guiderdoni, E., and Périn, C. (2011). Leucine-Rich repeat receptor kinases are sporadically distributed in eukaryotic genomes. BMC Evol. Biol. *11*, 367. https://doi.org/10.1186/1471-2148-11-367.

Dong, S., Yin, W., Kong, G., Yang, X., Qutob, D., Chen, Q., Kale, S.D., Sui, Y., Zhang, Z., Dou, D., et al. (2011). *Phytophthora sojae* avirulence effector Avr3b is a secreted NADH and ADP-ribose pyrophosphorylase that modulates plant immunity. PLoS Pathog. *7*, e1002353. https://doi.org/10.1371/journal.ppat.1002353.

Dou, D., and Zhou, J.-M. (2012). Phytopathogen effectors subverting host immunity: different foes, similar battleground. Cell Host Microbe *12*, 484–495. https://doi.org/10.1016/j.chom.2012.09.003.

El-Defrawy, M.M.H., and Hesham, A.E.-L. (2020). G-protein-coupled receptors in fungi. In Fungal Biotechnology and Bioengineering. Fungal Biology, A.L. Hesham, R. Upadhyay, G. Sharma, C. Manoharachary, and V. Gupta, eds. (Springer), pp. 37–126.

Fang, Y., and Tyler, B.M. (2016). Efficient disruption and replacement of an effector gene in the oomycete *Phytophthora sojae using* CRISPR/Cas9. Mol. Plant Pathol. *17*, 127–139. https://doi.org/10.1111/mpp.12318.

Fischer, I., Dievart, A., Droc, G., Dufayard, J.F., and Chantret, N. (2016). Evolutionary dynamics of the leucine-rich repeat receptor-like kinase (LRR-RLK) subfamily in angiosperms. Plant Physiol. *170*, 1595–1610. https://doi.org/10.1104/pp.15.01470.

Gao, G., Yin, D., Chen, S., Xia, F., Yang, J., Li, Q., and Wang, W. (2012). Effect of biocontrol agent *Pseudomonas fluorescens* 2P24 on soil fungal community in cucumber rhizosphere using T-RFLP and DGGE. PLoS One *7*, e31806. https://doi.org/10.1371/journal.pone.0031806.

Gao, J., Cao, M., Ye, W., Li, H., Kong, L., Zheng, X., and Wang, Y. (2015). PsMPK7, a stress-associated mitogen-activated protein kinase (MAPK) in *Phytophthora sojae*, is required for stress tolerance, reactive oxygenated species detoxification, cyst germination, sexual reproduction and infection of soybean. Mol. Plant Pathol. *16*, 61–70. https://doi.org/10.1111/mpp.12163.

Gisi, U., and Sierotzki, H. (2015). Oomycete fungicides: phenylamides, quinone outside inhibitors, and carboxylic acid amides. In Fungicide Resistance in Plant Pathogens, H. Ishii and D. Hollomon, eds. (Springer), pp. 145–174.

Gou, X., He, K., Yang, H., Yuan, T., Lin, H., Clouse, S.D., and Li, J. (2010). Genome-wide cloning and sequence analysis of leucine-rich repeat receptor-like protein kinase genes in *Arabidopsis thaliana*. BMC Genomics *11*, 19. https://doi.org/10.1186/1471-2164-11-19.

Gunderson, J.H., Elwood, H., Ingold, A., Kindle, K., and Sogin, M.L. (1987). Phylogenetic relationships between chlorophytes, chrysophytes, and oomycetes. Proc. Natl. Acad. Sci. *84*, 5823–5827. https://doi.org/10.1073/pnas.84.16.5823.

He, Y., Zhou, J., Shan, L., and Meng, X. (2018). Plant cell surface receptor-mediated signaling – a common theme amid diversity. J. Cell Sci. *131*, jcs209353. https://doi.org/10.1242/jcs.209353.

Hua, C., Wang, Y., Zheng, X., Dou, D., Zhang, Z., Govers, F., and Wang, Y. (2008). A *Phytophthora sojae* G-protein alpha subunit is involved in chemotaxis to soybean isoflavones. Eukaryot. Cell *7*, 2133–2140. https://doi.org/10.1128/EC.00286-08.

Jiang, R.H., and Tyler, B.M. (2012). Mechanisms and evolution of virulence in oomycetes. Annu. Rev. Phytopathol. *50*, 295–318. https://doi.org/10.1146/annurev-phyto-081211-172912.

Judelson, H.S., and Ah-Fong, A.M.V. (2019). Exchanges at the plant-oomycete interface that influence disease. Plant Physiol. *179*, 1198–1211. https://doi.org/10.1104/pp.18.00979.

Judelson, H.S., and Blanco, F.A. (2005). The spores of *Phytophthora*: weapons of the plant destroyer. Nat. Rev. Microbiol. *3*, 47–58. https://doi.org/10.1038/nrmicro1064.

Latijnhouwers, M., Ligterink, W., Vleeshouwers, V.G., van West, P., and Govers, F. (2004). A Galpha subunit controls zoospore motility and virulence in the potato late blight pathogen *Phytophthora infestans*. Mol. Microbiol. *51*, 925–936. https://doi.org/10.1046/j.1365-2958.2003.03893.x.

Li, A., Wang, Y., Tao, K., Dong, S., Huang, Q., Dai, T., Zheng, X., and Wang, Y. (2010). PsSAK1, a stress-activated MAP kinase of *Phytophthora sojae*, is required for zoospore viability and infection of soybean. Mol. Plant Microbe Interact. *23*, 1022–1031. https://doi.org/10.1094/MPMI-23-8-1022.

Li, A., Zhang, M., Wang, Y., Li, D., Liu, X., Tao, K., Ye, W., and Wang, Y. (2014). PsMPK1, an SLT2-type mitogen-activated protein kinase, is required for hyphal growth, zoosporogenesis, cell wall integrity, and pathogenicity in *Phytophthora sojae*. Fungal Genet. Biol. *65*, 14–24. https://doi.org/10.1016/j.fgb.2014.01.003.

Li, Q., Ai, G., Shen, D., Zou, F., Wang, J., Bai, T., Chen, Y., Li, S., Zhang, M., Jing, M., and Dou, D. (2019). A *Phytophthora capsici* effector targets ACD11 binding partners that regulate ROS-mediated defense response in *Arabidopsis*. Mol. Plant *12*, 565–581. https://doi.org/10.1016/j.molp.2019.01.018.

Li, Q., Zhang, M., Shen, D., Liu, T., Chen, Y., Zhou, J.-M., and Dou, D. (2016). A *Phytophthora sojae* effector PsCRN63 forms homo-/hetero-dimers to suppress plant immunity via an inverted association manner. Sci. Rep. *6*, 26951. https://doi.org/10.1038/srep26951.

Liang, X., Ding, P., Lian, K., Wang, J., Ma, M., Li, L., Li, L., Li, M., Zhang, X., Chen, S., et al. (2016). *Arabidopsis* heterotrimeric G proteins regulate immunity by directly coupling to the FLS2 receptor. Elife *5*, e13568. https://doi.org/10.7554/eLife.13568.

Ma, X., Claus, L.A.N., Leslie, M.E., Tao, K., Wu, Z., Liu, J., Yu, X., Li, B., Zhou, J., Savatin, D.V., et al. (2020). Ligand-induced monoubiquitination of BIK1 regulates plant immunity. Nature *581*, 199–203. https://doi.org/10.1038/s41586-020-2210-3.

Ma, Z., Song, T., Zhu, L., Ye, W., Wang, Y., Shao, Y., Dong, S., Zhang, Z., Dou, D., Zheng, X., et al. (2015). A *Phytophthora sojae* glycoside hydrolase 12 protein is a major virulence factor during soybean infection and is recognized as a PAMP. Plant Cell *27*, 2057–2072. https://doi.org/10.1105/tpc.15.00390.

Magalhaes, D.M., Scholte, L.L., Silva, N.V., Oliveira, G.C., Zipfel, C., Takita, M.A., and De Souza, A.A. (2016). LRR-RLK family from two Citrus species: genome-wide identification and evolutionary aspects. BMC Genomics *17*, 623. https://doi.org/10.1186/s12864-016-2930-9.

Man, J., Gallagher, J.P., and Bartlett, M. (2020). Structural evolution drives diversification of the large LRR-RLK gene family. New Phytol. *226*, 1492–1505. https://doi.org/10.1111/nph.16455.

Matson, M.E.H., Small, I.M., Fry, W.E., and Judelson, H.S. (2015). Metalaxyl resistance in *Phytophthora infestans*: assessing role of RPA190 gene and diversity within clonal lineages. Phytopathology® *105*, 1594–1600. https://doi.org/10.1094/PHYTO-05-15-0129-R.

Morris, P.F., Bone, E., and Tyler, B.M. (1998). Chemotropic and contact responses of *Phytophthora sojae* hyphae to soybean isoflavonoids and artificial substrates. Plant Physiol. *117*, 1171–1178. https://doi.org/10.1104/pp.117.4.1171.

Morris, P.F., and Ward, E.W.B. (1992). Chemoattraction of zoospores of the soybean pathogen, *Phytophthora sojae*, by isoflavones. Physiol. Mol. Plant Pathol. *40*, 17–22. https://doi.org/10.1016/0885-5765(92)90067-6.

Nitta, Y., Ding, P., and Zhang, Y. (2015). Heterotrimeric G proteins in plant defense against pathogens and ABA signaling. Environ. Exp. Bot. *114*, 153–158. https://doi.org/10.1016/j.envexpbot.2014.06.011.

Nolan, T., Chen, J., and Yin, Y. (2017). Cross-talk of Brassinosteroid signaling in controlling growth and stress responses. Biochem. J. *474*, 2641–2661. https://doi.org/10.1042/BCJ20160633.

O'Neill, L.A.J. (2004). TLRs: professor Mechnikov, sit on your hat. Trends Immunol. *25*, 687–693. https://doi.org/10.1016/j.it.2004.10.005.

Peng, Y., Chen, L., Li, S., Zhang, Y., Xu, R., Liu, Z., Liu, W., Kong, J., Huang, X., Wang, Y., et al. (2018). BRI1 and BAK1 interact with G proteins and regulate sugar-responsive growth and development in *Arabidopsis*. Nat. Commun. *9*,

1522. https://doi.org/10.1038/s41467-018-03884-8.

Qiu, M., Li, Y., Zhang, X., Xuan, M., Zhang, B., Ye, W., Zheng, X., Govers, F., and Wang, Y. (2020). G protein α subunit suppresses sporangium formation through a serine/threonine protein kinase in *Phytophthora sojae*. PLoS Pathog. *16*, e1008138. https://doi.org/10.1371/journal.ppat.1008138.

Safdar, A., Li, Q., Shen, D., Chen, L., He, F., Wang, R., Zhang, M., Mafurah, J.J., Khan, S.A., and Dou, D. (2017). An LRR receptor kinase regulates growth, development and pathogenesis in *Phytophthora capsici*. Microbiol. Res. *198*, 8–15. https://doi.org/10.1016/j.micres.2017.01.008.

Shiu, S.H., and Bleecker, A.B. (2003). Expansion of the receptor-like kinase/Pelle gene family and receptor-like proteins in *Arabidopsis*. Plant Physiol. *132*, 530–543. https://doi.org/10.1104/pp.103.021964.

Shiu, S.-H., and Bleecker, A.B. (2001a). Plant receptor-like kinase gene family: diversity, function, and signaling. Sci. STKE *2001*, re22. https://doi.org/10.1126/stke.2001.113.re22.

Shiu, S.H., and Bleecker, A.B. (2001b). Receptor-like kinases from *Arabidopsis* form a monophyletic gene family related to animal receptor kinases. Proc. Natl. Acad. Sci. U S A *98*, 10763–10768. https://doi.org/10.1073/pnas.181141598.

Smakowska-Luzan, E., Mott, G.A., Parys, K., Stegmann, M., Howton, T.C., Layeghifard, M., Neuhold, J., Lehner, A., Kong, J., Grünwald, K., et al. (2018). An extracellular network of *Arabidopsis* leucine-rich repeat receptor kinases. Nature *553*, 342–346. https://doi.org/10.1038/nature25184.

Snelders, N.C., Rovenich, H., Petti, G.C., Rocafort, M., van den Berg, G.C.M., Vorholt, J.A., Mesters, J.R., Seidl, M.F., Nijland, R., and Thomma, B.P.H.J. (2020). Microbiome manipulation by a soil-borne fungal plant pathogen using effector proteins. Nat. Plants *6*, 1365–1374. https://doi.org/10.1038/s41477-020-00799-5.

Soanes, D.M., and Talbot, N.J. (2010). Comparative genome analysis reveals an absence of leucine-rich repeat pattern-recognition receptor proteins in the kingdom Fungi. PLoS One *5*, e12725. https://doi.org/10.1371/journal.pone.0012725.

Song, W., Han, Z., Wang, J., Lin, G., and Chai, J. (2017). Structural insights into ligand recognition and activation of plant receptor kinases. Curr. Opin. Struct. Biol. *43*, 18–27. https://doi.org/10.1016/j.sbi.2016.09.012.

Syed-Ab-Rahman, S.F., Carvalhais, L.C., Chua, E., Xiao, Y., Wass, T.J., and Schenk, P.M. (2018). Identification of soil bacterial isolates suppressing different *Phytophthora spp.* and promoting plant growth. Front. Plant Sci. *9*, 1502. https://doi.org/10.3389/fpls.2018.01502.

Tang, D., Wang, G., and Zhou, J.M. (2017). Receptor kinases in plant-pathogen interactions: more than pattern recognition. Plant Cell *29*, 618–637. https://doi.org/10.1105/tpc.16.00891.

Thines, M. (2014). Phylogeny and evolution of plant pathogenic oomycetes—a global overview. Eur. J. Plant Pathol. *138*, 431–447. https://doi.org/10.1007/s10658-013-0366-5.

Tomada, S., Sonego, P., Moretto, M., Engelen, K., Pertot, I., Perazzolli, M., and Puopolo, G. (2017). Dual RNA-Seq of Lysobacter capsici AZ78 – *Phytophthora infestans* interaction shows the implementation of attack strategies by the bacterium and unsuccessful oomycete defense responses. Environ. Microbiol. *19*, 4113–4125. https://doi.org/10.1111/1462-2920.13861.

Tyler, B.M. (2007). *Phytophthora sojae*: root rot pathogen of soybean and model oomycete. Mol. Plant Pathol. *8*, 1–8. https://doi.org/10.1111/j.1364-3703.2006.00373.x.

Tyler, B.M., Tripathy, S., Zhang, X., Dehal, P., Jiang, R.H., Aerts, A., Arredondo, F.D., Baxter, L., Bensasson, D., Beynon, J.L., et al. (2006). *Phytophthora* genome sequences uncover evolutionary origins and mechanisms of pathogenesis. Science *313*, 1261–1266. https://doi.org/10.1126/science.1128796.

van der Geer, P., Hunter, T., and Lindberg, R.A. (1994). Receptor protein-tyrosine kinases and their signal transduction pathways. Annu. Rev. Cell Biol. *10*, 251–337. https://doi.org/10.1146/annurev.cb.10.110194.001343.

Vrieze, M.D., Gloor, R., Codina, J.M., Torriani, S., Gindro, K., L'Haridon, F., Bailly, A., and Weisskopf, L. (2019). Biocontrol activity of three *Pseudomonas* in a newly assembled collection of *Phytophthora infestans* isolates. Phytopathology *109*, 1555–1565. https://doi.org/10.1094/PHYTO-12-18-0487-R.

Wagner, A., Norris, S., Chatterjee, P., Morris, P.F., and Wildschutte, H. (2018). Aquatic pseudomonads inhibit oomycete plant pathogens of *Glycine max*. Front. Microbiol. *9*, 1007. https://doi.org/10.3389/fmicb.2018.01007.

Wang, J., Shen, D., Ge, C., Du, Y., Lin, L., Liu, J., Bai, T., Jing, M., Qian, G., and Dou, D. (2020). Filamentous *Phytophthora* pathogens deploy effectors to interfere with bacterial growth and motility. Front. Microbiol. *11*, 581511. https://doi.org/10.3389/fmicb.2020.581511.

Wang, W., Liu, D., Zhuo, X., Wang, Y., Song, Z., Chen, F., Pan, Y., and Gao, Z. (2021). The RPA190-pc gene participates in the regulation of metalaxyl sensitivity, pathogenicity and growth in *Phytophthora capsici*. Gene *764*, 145081. https://doi.org/10.1016/j.gene.2020.145081.

Wu, L., Huang, Z., Li, X., Ma, L., Gu, Q., Wu, H., Liu, J., Borriss, R., Wu, Z., and Gao, X. (2018). Stomatal closure and SA-, JA/ET-Signaling pathways are essential for *Bacillus amyloliquefaciens* FZB42 to restrict leaf disease caused by *Phytophthora nicotianae* in *Nicotiana benthamiana*. Front. Microbiol. *9*, 847. https://doi.org/10.3389/fmicb.2018.00847.

Ye, W., Wang, X., Tao, K., Lu, Y., Dai, T., Dong, S., Dou, D., Gijzen, M., and Wang, Y. (2011). Digital gene expression profiling of the *Phytophthora sojae* transcriptome. Mol. Plant Microbe Interact. *24*, 1530–1539. https://doi.org/10.1094/mpmi-05-11-0106.

Zhang, M., Su, J., Zhang, Y., Xu, J., and Zhang, S. (2018). Conveying endogenous and exogenous signals: MAPK cascades in plant growth and defense. Curr. Opin. Plant Biol. *45*, 1–10. https://doi.org/10.1016/j.pbi.2018.04.012.

Zhang, X., Jiang, H., and Hao, J. (2019). Evaluation of the risk of development of fluopicolide resistance in *Phytophthora erythroseptica*. Plant Dis. *103*, 284–288. https://doi.org/10.1094/PDIS-02-18-0366-RE.

Zhang, X., Zhai, C., Hua, C., Qiu, M., Hao, Y., Nie, P., Ye, W., and Wang, Y. (2016). PsHint1, associated with the G-protein alpha subunit PsGPA1, is required for the chemotaxis and pathogenicity of *Phytophthora sojae*. Mol. Plant Pathol. *17*, 272–285. https://doi.org/10.1111/mpp.12279.

Zhou, J.-M., and Zhang, Y. (2020). Plant immunity: danger perception and signaling. Cell *181*, 978–989. https://doi.org/10.1016/j.cell.2020.04.028.

STAR★METHODS

KEY RESOURCES TABLE

REAGENT or RESOURCE	SOURCE	IDENTIFIER
Antibodies		
His-Tag (2A8) Antibody	Abmart	Cat# M20001L
GST-Tag(12G8) Mouse Antibody	Abmart	Cat# M20007L; RRID:AB_2864360
GFP-Tag(7G9) Mouse Antibody	Abmart	Cat# M20004L; RRID:AB_2619674
DYKDDDDK-Tag(3B9) Mouse Antibody	Abmart	Cat# M20008L; RRID:AB_2713960
IRDye 800CW Goat anti-Mouse IgG Secondary Antibody	Li-COR	Cat# 926-32210; RRID:AB_621842
Bacterial and virus strains		
Escherichia coli DH5a	Sangon Biotech	Cat# B528413
Escherichia coli Rosetta (DE3)	Sangon Biotech	Cat# B528422
Agrobacterium tumefaciens GV3101	TOLOBIO	Cat# 96305-01
Bacillus amyloliquefaciens FZB42	(Wu et al., 2018)	N/A
Pseudomonas fluorescens 2P24	(Gao et al., 2012)	N/A
Chemicals, peptides, and recombinant proteins		
GFP-Trap_A	Chromotek	Cat# gta-100
Glutathione Sepharose 4 (affinity gel)	Thermo Fisher Scientific	Cat# 16100
Amylose Resin	NEB	Cat# 50-811-582
Lysing enzymes from *Trichoderma harzianum*	Sigma	Cat# L1412
CELLULYSIN Cellulase, *Trichoderma viride*	Calbiochem	Cat# 219466
D-Luciferin, Potassium Salt	Warbio	Cat# Y302C
Isoflavones	Sigma	Cat# 43534
Metalaxyl	(Matson et al., 2015)	N/A
Fluopicolide	(Zhang et al., 2019)	N/A
3,3′-diaminobenzidine (DAB)	Sigma	Cat# D8001
Critical commercial assays		
pIMAGO-HRP Phosphoprotein Detection on Western Blot	TYMORA	Cat# 79464
PureLink RNA mini kit	Invitrogen	Cat# 12183020
ChamQ SYBR qPCR Master Mix	Vazyme	Cat# Q311-03
Experimental models: Organisms/strains		
For all Δ*PsRLK* mutants generated in this study	This paper	N/A
Oligonucleotides		
For all oligonucleotides used for genotyping and cloning	See Table S3	N/A
Recombinant DNA		
GST-PsRLK5/11/17/22/24^{KD} (*E. coli* expression)	This paper	N/A
PsGPA1-His (*E. coli* expression)	This paper	N/A
MBP-PsRLK5/11/17/22/24^{KD} (*E. coli* expression)	This paper	N/A
GST-BIK1 (*E. coli* expression)	Ma et al. (2020)	N/A

(*Continued on next page*)

Continued

REAGENT or RESOURCE	SOURCE	IDENTIFIER
Software and algorithms		
Prism 8	GraphPad Software	RRID:SCR_002798
ImageJ	Schneider et al., 2012	https://imagej.nih.gov/ij/
Odyssey® CLX Imaging System	LI-COR	https://www.licor.com/bio/odyssey-clx/
Excl	Microsoft	N/A

RESOURCE AVAILABLE

Lead contact

Further information and requests for resources and reagents should be directed to and will be fulfilled by the lead contact, Daolong Dou (ddou@njau.edu.cn)

Materials availability

Materials generated in this study are available from the lead contact with a completed Materials Transfer Agreement.

Data and code availability

This study did not generate datasets.

EXPERIMENTAL MODEL AND SUBJECT DETAILS

Nicotiana benthamiana

N. benthamiana was grown in growth chamber at 22°C under a long-day photoperiod (16-h light and 8-h dark) throughout the experiment.

Glycine max

The soybean ecotype Hefeng 35 was used as the susceptible cultivar. Soybean seeds were grown in plastic pots containing vermiculite at 25°C in the dark for 4 days to generate etiolated seedlings.

Bacterial strains

Bacillus amyloliquefaciens FZB42 was cultivated in Luria-Bertani (LB) broth at 37°C with appropriate antibiotic. *Pseudomonas fluorescens* 2P24 was cultivated at 28°C in LB broth with appropriate antibiotic.

Phytophthora strains

The strains used in this study include *P. sojae* isolate P6497 and the PsRLKs knockout mutants used in this study were grown on 10% (vol/vol) vegetable juice (V8) agar medium at 25°C in the dark. The growth rate of each transformants was assayed on V8 plates and the colony diameters were measured after growth for 5 days. For stress response assays, 6 mM H_2O_2, 0.125 μg/mL metalaxyl or 0.15 μg/mL fluopicolide was included in V8 agar medium. Fresh 5×5-mm hyphal plugs were inoculated on V8 medium plates. Colony diameters were measured by fine crosshair and photographs were taken after 7 days. Inhibition rates were calculated using the following formula: inhibition rate = (growth rate on plates without stress – growth rate on plates with stress) / growth rate on plates without stress.

METHOD DETAILS

Bioinformatics analysis of LRR-RLKs

The genomes of representative species across eukaryote were initially retrieved from JGI and NCBI databases. To predict LRR-RLK proteins in each genome, the Hidden Markov Model (HMM) profiles of LRR domains including LRR_1 (PF00560), LRR_2 (PF07723), LRR_3 (PF07725), LRR_4 (PF12799), LRR_5 (PF13306), LRR_6 (PF13516), LRR_8 (PF13855), and LRR_9 (PF14580) were obtained from PFAM database (pfam.xfam.org), followed by searching against each genome using HMMER pipeline (E value cut-off < 1). The HMM profile of KD (PF00069) was also searched (E value cutoff < 1e-5). The TM was predicted using TMHMM Server (www.cbs.dtu.dk/services/TMHMM). Proteins containing at least one LRR domain, a TM,

and a KD were then considered to be putative LRR-RLK protein. To analyze the phylogenetic relationships of LRR-RLKs between oomycetes and plants, all the predicted LRR-RLKs in oomycetes and the representative subgroup member of *A. thaliana* were used to construct the phylogenetic tree following the neighbor-joining algorithm with 1,000 bootstrap replicates using MEGA7 software. To estimate the numbers of LRR-RLKs in the ancestral species and gains and losses of genes during evolution, the modified reconciled-tree method was performed by comparing the bootstrap condensed gene tree with the species tree under the parsimony principle. The residues of each LRR domain were extracted and residue logos of each LRR were visualized with WebLogo (http://weblogo.threeplusone.com/).

Generation of PsRLK-knockout mutants

All gene deletion mutants were generated with CRISPR-mediated gene replacement strategy (Fang and Tyler, 2016). sgRNA oligonucleotides targeting PsRLK genes were cloned into the pYF515 vector, which harbors both the Cas9 and the sgRNA cassettes. The *NPT II* gene was ligated with two homologous fragments of the targeted PsRLK gene individually and used as the donor DNA in homology-directed repair. Constructs harboring NPT II and Cas9/sgRNA were then cotransformed into *P. sojae* using PEG-mediated protoplast transformation. Putative transformants were screened on V8 agar medium containing 50 μg/mL geneticin (G418). Resistant clones were checked by genomic PCR using PsRLK-specific primers to confirm deletion. Then the recombinant inserts were sequenced. For the generation of *ΔPsRLK21&10* and *ΔPsRLK21&17* double mutants, *PsRLK21* knockout mutant was used as the recipient strain for knocking out *PsRLK10* or *PsRLK21*.

Biocontrol bacteria treatments

Bacillus amyloliquefaciens FZB42 was cultivated in LB broth at 37°C until the OD600 reached 2.0. *Pseudomonas fluorescens* 2P24 was cultivated at 28°C until the OD600 reached 1.5. Each *P. sojae* strain was grown in the middle of V8 plates and incubated at 25°C in the dark for two days before adding biocontrol bacteria. Then, two holes were made using sterile tips (6 mm in diameter) which were 1.5 cm away from the central point of the quantitative V8 agar medium (7 cm in diameter). 25 μL preheated LB medium was added to each hole and allowed to solidify. Then, 5 μL bacteria solution of FZB42 was dropped on the right hole, while 5 μL sterile ddH_2O was dropped on the left as a control. 2P24 treatment was performed the same way except that it was applied 24 h after mycelial growth. Non-treatment mycelial was set as a control. Photographs were taken 4 and 5 days after treatments of FZB42 and 2P24, respectively. The experiments were independently repeated three times.

Zoospore and sporangium production assays

To quantify zoospore production, three round mycelial disks (6 mm in diameter) cut from the same culture were inoculated to 10 mL of 10% V8 broth and cultured for 3 days in the dark. Sporangia or zoospores were prepared by repeatedly washing mycelia with sterile water every 30 min and incubating in 5 ml of water at 25°C for about 8 h until most mycelia developed sporangia. Zoospores were then released. Sporangia were subsequently mixed gently with a blender to obtain a homogenous mixture. Three random 100-μL samples were examined under microscope at 10 × magnification to calculate the number of sporangia in each sample. When most zoospores were released, their numbers were counted in 100-μL suspension samples using hemocytometer. All assays were independently repeated for at least 3 times and the significance of difference was tested by ANOVA.

Zoospore chemotaxis assays

To examine the chemotaxis of zoospores towards isoflavones, 1% agarose gel containing 15 μM isoflavones were cut into 2×2-mm pieces and placed in the chambers. 60 μL diluted zoospore fluid (10^4 zoospores per milliliter) was dripped in the middle of the chamber. After treatment for 3 min and 6 min, photographs were taken under a microscope to examine the dispersion state of zoospores. Zoospore numbers were calculated by ImageJ. All assays were repeated at least 3 times.

In another chemotaxis assay, zoospores suspensions were inoculated onto water agar at a central scoring line with two parallel wells (10 mm away) on both sides filled with 15 μM isoflavones or the solvent control. After 5 min, zoospores swam towards the isoflavones (Σisof) or the solvent (Σsolv) were counted to calculate the chemotrophic index as (Σtotal − Σsolv) / Σtotal × 100 in which Σtotal is the total number of zoospores counted. The assay was repeated at least 5 times for each strain.

Protein-protein interaction assays

LCI assay vectors pCAMBIA1300-Nluc and pCAMBIA1300-Cluc were generously provided by Prof. Jian-Min Zhou. Both Nluc and Cluc fusions are located at the C-terminal of fused protein. The LCI procedure has been previously described (Chen et al., 2008). Full-length and KD sequences of *PsRLK5/11/17/22/24* were individually expressed with Cluc fusion, while *PsGPA1* was fused with Nluc. Individual PsRLK-Cluc, PsRLK^{KD}-Cluc and PsGPA1-Nluc constructs were electrically transformed into *Agrobacterium tumefaciens* strain GV3101. The XLG2-Nluc and FLS2-Cluc combination was used as a positive control. For agroinfiltrations, *Agrobacterium* cultures harboring Cluc- and Nluc-fusion proteins were mixed and injected into *N. benthamiana* leaves. Each combination was repeated in 6 leaves. Fluorescence was generated by spraying D-Luciferinon on the leaves 36 to 48 h after infiltration. Same LCI method was used for exploring the interaction network of PsRLKs.

For the Co-IP assay in *N. benthamiana*, FLAG and GFP-tagged proteins were coexpressed via agroinfiltration. Total proteins were extracted from infiltrated leaves by incubating the ground leaf samples in extraction buffer containing 150–200 mM NaCl, 50 mM Tris-HCl (pH 7.5), 10 mM ethylenediaminetetraacetic acid, 1.0% (v/v) NP-40, 1 mM phenylmethylsulfonyl fluoride, and 0.1% (v/v) protease inhibitor cocktail (P9599; Sigma, St. Louis, MI, USA) for 20 min. After centrifuged at 13,000×g for 15 min, the supernatant was incubated with GFP-trap A beads (Chromotek, Hauppauge, NY, USA, gta-100) at 4°C for 4 h. The beads were pelleted and washed with extraction buffer for three times. Coimmunoprecipitated proteins were then eluted and analyzed by Western blots using 1:5000 diluted anti-FLAG (Abmart, Berkeley Heights, NJ, USA, M20004L) and anti-GFP (Abmart, Berkeley Heights, NJ, USA, M20004L) antibodies followed by incubation with 1:10,000 diluted goat antimouse (irdye 800, 926-32210; LI-COR Biosciences, Lincoln, NE, USA) antibody. The blots were visualized using the Odyssey CLX Imaging System.

For yeast two-hybrid (Y2H) assay, the indicated plasmid combinations were cotransformed into yeast and positive clones were selected on SD/-Leu/-Trp medium. Subsequently, randomly selected clones were transferred to SD/-Leu/-Trp/-His medium for growth analysis.

For *in vitro* GST pull-down assay, GST- and His-tagged candidate interacting proteins were expressed in *E. coli* Rosetta (DE3) strain. The Glutathione Sepharose™ 4B Media used for GST pull-down was pretreated by 1×TBST before co-incubating with GST-fusion protein. 1 mL GST-fusion protein extract supernatant was incubated with 50 μL beads working solution (containing 25 μL glutathione agarose beads) for 4 h. The mixture was then centrifuged, and the supernatant was abandoned carefully before adding His-fusion protein to coincubate for another 4 h. After that, the beads were washed three times and boiled with loading buffer for 10 min. The pull-down of His-fusion protein was detected by Western blot with anti-His antibody.

In vitro phosphorylation assays

The PsRLK5/11/17/22/24^{KD} was cloned as maltose-binding protein fusions for recombinant protein expression in *E. coli* Rosetta (DE3) strain. The protein expression was induced by addition of 0.1 mM IPTG to 200 mL culture at OD600 = 0.5, followed by incubation at 18°C for 12 h. Cells were harvested and resuspended in TBST buffer, followed by lysis using a microfluidizer. Cell lysates were centrifuged at 12000 g to separate insoluble cell debris and purified using amylose resin beads (NEB). GST-BIK1 was expressed and purified as previously described (Ma et al., 2020). The purified recombinant proteins were directly subjected to autophosphorylation examination using the pIMAGO-biotin phosphoprotein detection kit (Tymora) as per the manufacturer's instructions.

RNA extraction and gene expression analysis

Total RNAs of zoospores from the indicated strains were extracted using a PureLink RNA mini kit (Invitrogen, Carlsbad, CA, USA). All RNA samples were then treated with DNase I to remove potential DNA contamination. Approximately 1 μg RNA was used for reverse transcription with oligo (dT) primers. Then, the cDNA reaction mixture was diluted 5 times and 2 μL was used as the template in a 20 μL PCR reaction with SYBR qPCR Master Mix (Vazyme). qPCR was performed using an ABI Prism 7500 Fast Real-Time PCR system as per the manufacturer's instructions. Relative transcript amount differences were calculated using the 2-ΔCT method in ABI 7500 System Sequence Detection Software. Three biological replicates were performed and the results showed similar trends. The expression levels of PsGPA1 in the indicated strains and the expression of PsRLKs under biocontrol bacteria treatments were determined by qRT-PCR. Relative gene expression levels were determined using actin as the internal control.

Virulence assays

Zoospores were induced as described previously and diluted to a concentration of 200 zoospores/10 μL. Etiolated seedlings were inoculated by pipetting 10 μL of the zoospore suspension on the hypocotyls and then grown at 25°C in a dark incubator with 80% relative humidity. For soybean root-dipping inoculation with zoospores, the root of 4-day-old etiolated seedlings was dipped for 30 min in suspension of 10^5 zoospores mL^{-1} and subsequently grown at 25°C with 80% relative humidity. Lesions were evaluated and photographed at 2 dpi. Virulence was also quantified by calculating the ratio of *P. sojae* DNA to soybean DNA in infected soybean, as measured by qRT-PCR.

To examining ROS levels in infected soybean, *P. sojae*-inoculated seedlings were collected at 36 h and soaked into 1 mg/ml DAB for 8 h. After de-staining in an ethanol/acetic acid solution (47:1 [vol/vol]) for 4 h, infected epidermis cells were examined and photographed under a microscope. DAB-stained cells were then counted. Each strain was tested using five seedlings and at least two different preparations of zoospores. All assays were repeated at least three times.

QUANTIFICATION AND STATISTICAL ANALYSIS

Error bars of the graphs represent the mean value ± standard deviation (SD). To compare two different groups, Student's t-test was used as the parametric test. To compare multi groups, one-way ANOVA with Dunnett's multiple-comparison test was performed to compare means from several groups against a control group mean. Statistical analysis was performed using Microsoft Excel 2019 and Prism 8 software (GraphPad).